

The Solar Irradiance Spectrum at Solar Activity Minimum Between Solar Cycles 23 and 24

G. Thuillier · D. Bolsée · G. Schmidtke · T. Foujols · B. Nikutowski · A.I. Shapiro · R. Brunner · M. Weber · C. Erhardt · M. Hersé · D. Gillotay · W. Peetermans · W. Decuyper · N. Pereira · M. Haberreiter · H. Mandel · W. Schmutz

Received: 16 May 2013 / Accepted: 6 December 2013 / Published online: 28 December 2013
© Springer Science+Business Media Dordrecht 2013

Abstract On 7 February 2008, the SOLAR payload was placed onboard the *International Space Station*. It is composed of three instruments, two spectrometers and a radiometer. The two spectrometers allow us to cover the 16–2900 nm spectral range. In this article, we first briefly present the instrumentation, its calibration and its performance in orbit. Second, the solar spectrum measured during the transition between Solar Cycles 23 to 24 at the time of the minimum is shown and compared with other data sets. Its accuracy is estimated as a function of wavelength and the solar atmosphere brightness-temperature is calculated and compared with those derived from two theoretical models.

Keywords Solar spectrum · Solar minimum · Space Station · SolACES · SOLSPEC

G. Thuillier (✉) · T. Foujols · M. Hersé
LATMOS-CNRS, 11 Blvd d'Alembert, 78280 Guyancourt, France
e-mail: gerard.thuillier@latmos.ipsl.fr

D. Bolsée · D. Gillotay · W. Peetermans · W. Decuyper · N. Pereira
Institut d'Aéronomie Spatiale de Belgique, 3 avenue Circulaire, 1180 Brussels, Belgium

G. Schmidtke · B. Nikutowski · R. Brunner · C. Erhardt
Fraunhofer Institute for Physical Measuring Technique, Heidenhofstrasse 8, 79110 Freiburg, Germany

B. Nikutowski
Institute for Meteorology, University of Leipzig, Stephanstr. 3, 04103 Leipzig, Germany

A.I. Shapiro · M. Haberreiter · W. Schmutz
Physikalisch-Meteorologisches Observatorium Davos, World Radiation Center, 7260 Davos Dorf, Switzerland

M. Weber
Institute of Environmental Physics (IUP), University of Bremen FB1, Otto-Hahn-Allee 1, 28359 Bremen, Germany

H. Mandel
Landessternwarte, Königstuhl, Heidelberg, Germany

1. Introduction

1.1. The Birth of the SOLAR Payload

In the 1990s, the interest to know the solar spectral irradiance (SSI) in a large spectral domain led the community to consider missions that could obtain measurements from the extreme-ultraviolet (EUV) to the infrared (IR). This scientific interest was based on solar, atmospheric, and climate physics. For the latter, it has been suggested that the dynamical coupling between troposphere and upper atmosphere is an amplifying mechanism of the solar influence on the climate (see for example Meehl *et al.*, 2009). Furthermore, these measurements allowed us to resume EUV measurements after about 20 years. Moreover, simultaneously measuring the SSI and the total solar irradiance (TSI) would enable one to accurately study the role of the SSI variation with respect to the TSI variation, and to extend the TSI time series of the *Solar Heliospheric Observatory* (SOHO) radiometers. An announcement of opportunity was released by the European Space Agency (ESA), soliciting proposals associated with the *Columbus* laboratory.

Three instruments were selected by the ESA Microgravity and Space Station Utilisation Department following the evaluation of the ESA announcement of opportunity for Externally Mounted Payloads (SP-1201):

- the *Solar Variability Irradiance Monitor* (SOVIM),
- the *Solar Auto-Calibrating EUV/UV Spectrometers* (SolACES), and
- the *Solar Spectrum* (SOLSPEC).

These three instruments were developed under the responsibility of the Physikalisch-Meteorologisches Observatorium Davos/World Radiation Center (Switzerland), the Fraunhofer Institute for Physical Measuring Technique (Germany), and the Laboratoire Atmosphères, Milieux, Observations Spatiales-Centre National de la Recherche Scientifique (France), respectively.

The three instruments were chosen because of the consistency of their measurements, and the mission was named SOLAR. SOVIM and SOLSPEC were partially hardware reflights. They were placed on the *Coarse Pointing Device* (CPD), ensuring a solar viewing independently of the *International Space Station* (ISS) movements. The original date for launch was planned for 2002, allowing measurements of the solar spectral irradiance during the descending phase of Solar Cycle 23. Because the mission development was slow for various reasons, the project was further delayed after the *Space Shuttle Columbia* disaster, which occurred on 1 February 2003. Finally, the three instruments on the CPD were launched with the *Columbus* module on 7 February 2008 and installed on the *External Payload Facility*. At the time of launch, the Sun was close to minimum activity. Finally, instead of measuring the SSI during the descending phase of Cycle 23, SOLAR measured during the solar minimum between Cycles 23 and 24 and during the ascending phase of Cycle 24.

Other solar missions in space are the following:

- The *Solar Radiation and Climate Experiment* (SORCE: Rottman, 2005) mission was launched in January 2003. The instrumentation consists of three spectrometers: the *Solar Stellar Irradiance Comparison Experiment* (SOLSTICE, working in the range 115–320 nm), the *Solar Irradiance Monitor* (SIM, 200–2400 nm) domain with a separate channel from 200–310 nm to overlap with SOLSTICE, the *XUV Photometer System* (XPS, 0.1–34 nm and Ly α). SORCE also carries an absolute radiometer to measure the total solar irradiance.

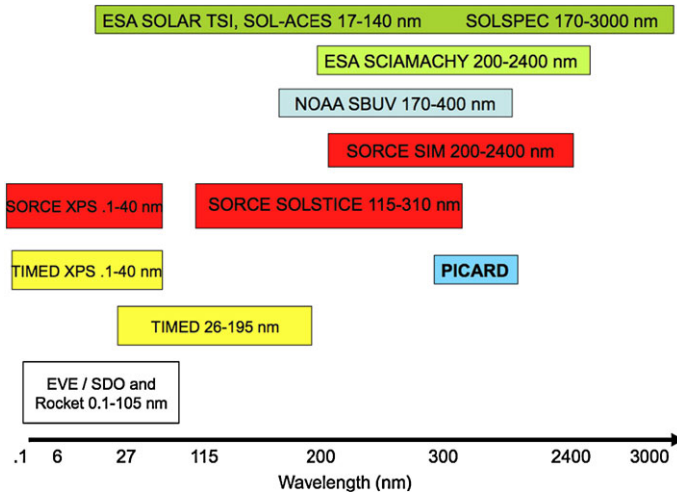


Figure 1 The different missions currently in space as a function of wavelength.

- In the EUV range, the *Thermosphere Ionosphere Mesosphere Energetics and Dynamics* satellite (TIMED: Woods *et al.*, 2005), launched on 7 December 2001, operates in the range 0.1 – 194 nm. Onboard the *Solar Dynamic Observatory* (SDO), the solar *EUV Experiment* (EVE: Crotser *et al.*, 2007; Woods *et al.*, 2010) measures the EUV spectral irradiance, while the *Atmosphere Imager Assembly* (AIA) provides images in that domain. Before the SDO mission, NASA launched a rocket on 14 April 2008 that carried the EVE instrument prototype to ensure the accuracy of the EUV absolute spectral irradiance to be measured by EVE onboard SDO. Onboard *Picard*, launched on 15 June 2010, the TSI, the UV, and the visible spectral irradiance are measured in some domains (Schmutz *et al.*, 2009). Missions in space are shown in Figure 1 as a function of wavelength.
- The *Scanning Imaging Absorption Spectrometer for Atmospheric Chartography* (SCIAMACHY: Bovensmann *et al.*, 1999) is a spectrometer that observes from 200 to 2400 nm. It is in operation since 2002 onboard the *Environment Satellite* (ENVISAT) platform. We briefly discuss the limitations of SCIAMACHY data. This instrument is equipped with a White Light Source (WLS) for photometric corrections, but can also be used for onboard ageing control. Pagarán *et al.* (2011) indicated, however, that the ageing of the lamps prevented its use after 2004. This is why we preferred using a spectrum from 2 August 2002, shortly after its launch, which is still reliable, for corrections. However, one should be aware that the SCIAMACHY UV spectrum taken near solar maximum will differ from the solar minimum UV spectra because of the solar-activity variability. However, in the visible and IR range, where the solar-cycle variability effect is likely well below 1 %, comparisons with SCIAMACHY are appropriate. Owing to the fairly low signal-to-noise ratio in the near-IR, SCIAMACHY channels (1900 nm, and 2400 nm) have an estimated accuracy of about 10 %. SCIAMACHY does not observe from 1761.7 to 1936.4 nm and from 2042.3 to 2260.7 nm because of the saturation effect of atmospheric water vapour when SCIAMACHY is taking Earth atmosphere measurements.

The SOLAR mission instruments onboard the ISS were initially developed for a period of operation of 18 months. When the manufacturing was almost completed, the SOLAR mission was extended to three years. After three years in space, the mission was again ex-

tended until the end of 2013, and finally to February 2017. This will allow us to study the decreasing phase of Solar Cycle 24.

1.2. Scientific Objectives

The SOLAR missions have different scientific objectives, from solar to atmospheric and climate physics. They have been described in detail by Schmidtke, Fröhlich, and Thuillier (2006) and Schmidtke *et al.* (2006):

- Solar physics: The solar spectrum characterizes the outer layers (photosphere, chromosphere, transition region, corona) of the Sun, and provides information about the composition and temperature of these regions. Furthermore, by comparison with theoretical reconstructions, an accurately measured spectrum allows us to validate the solar atmosphere properties and in particular the predictions, either theoretically or empirically, made for solar activity changes on TSI and SSI. Because the Sun is a variable star, TSI and SSI vary. Consequently, it is necessary to observe the effects of the appearance and disappearance of the active regions, as well as the long-term time variations, and have overlapping missions to ensure continuity. Accurate SSI measurements are also important for the SSI reconstructions based on theoretical approaches and proxies. These reconstructions can be validated by comparing them with measurements. The better the measurements, the better the model validation by pointing out possible defects. We employed the Code for Spectral Irradiance (COSI) modelling (Haberreiter, Schmutz, and Hubeny, 2008; Shapiro *et al.*, 2010) and the Solar Radiation Physical Modelling (SRPM: Fontenla *et al.*, 2011) to compare a theoretical approach with measurements.
- Atmospheric physics: The physical properties of the planetary atmospheres are primarily controlled by the solar radiation that induces the following main processes: photodissociation of molecules; recombination, which creates new species; ionization of molecules and atoms; excitation of these species; excitation of molecules and atoms by collisions with photoelectrons and suprathermal electrons; photon absorption, which leads to warming of the medium through fluorescence; and Rayleigh and resonant scattering while escaping radiation is re-distributing the solar energy. All these processes are wavelength dependent. Therefore, atmospheric modelling requires solar spectral irradiance from EUV to IR with an absolute accuracy compatible with the accuracy of the modelling capability. In other terms, the highest possible accuracy of the measurements is needed given the improvements made in atmospheric modelling. Furthermore, because solar cycles are not identical in their development, it is necessary to know the SSI for the time at which atmospheric physics data were collected.
- Climate physics: Processes involving changes driven by the Sun on atmospheric parameters are accepted today as possible actors in rapid climate changes. Climate models require solar spectra corresponding to different solar-activity regimes extending from UV to IR. This information is used to reconstruct the past SSI and TSI as a reference to which some spectral variability is applied based on chosen proxies. Currently, reconstructions do not have the required accuracy to reproduce the different SSI levels of solar activity. For example, to simulate the SSI at the Dalton minimum, the solar-activity minimum that occurred in 2008 and the corresponding data provide useful information for determining the SSI prediction accuracy. That is why the very low SSI observed in 2008 has received significant interest from several fields.

Section 2 briefly describes the SOLAR mission instruments and their performance in orbit. Section 3 is dedicated to the activity minimum that occurred in 2008 and to the construction of the SOLAR spectrum using SolACES and SOLSPEC data, including their photometric properties by comparing them with other spectra that were either measured or derived theoretically.

2. Brief Description of the Instrument Characteristics and Observations

2.1. The SolACES Spectrometer

SolACES (Schmidtke, Fröhlich, and Thuillier, 2006; Schmidtke *et al.*, 2006; 2013) records the solar EUV irradiance from 16 nm to 150 nm with a spectral resolution that is wavelength dependent, namely 0.3 nm below 65 nm, 0.4 nm between 65 and 100 nm, and 0.6 nm above. On top of the three grazing-incidence planar-grating spectrometers (SP) and on the two three-signal double-ionization chambers (IC), a filter wheel places a series of band-pass filters onto the SP and IC entrances, respectively. The actual transmission of the filters is measured by the following method:

The currents generated by the absorption of the transmitted EUV photons in the ionization chambers provide the data sets from which the corresponding absolute photon fluxes are derived. For each of these calibration measurements the ICs are refilled with gas. The calibration of the spectrometers is achieved by modelling the IC currents and bringing them into agreement with the measurements using several spectral subrange domains. The EUV wavelength range is covered by using different filters. For example, by selecting four different filters for the same spectral domain, two gases (neon and xenon) with different wavelength absorption range, and generating three currents in each of the ICs, 24 possibilities exist to cross-check the spectral irradiance in this spectral domain.

For the repeated in-flight calibration, a dependence on wavelength was measured. An uncertainty of 10 % was found for the wavelength range between 16 nm to around 50 nm. For the spectral region 90–150 nm, the mean uncertainty is 15 %. However, there is some uncertainty that reaches 20 % in some narrow spectral ranges. The details of this analysis are given in Schmidtke *et al.* (2013).

By operating the ionization chambers several times *per day*, a high degree of reliability is achieved for determining the temporal efficiency changes inherent to the EUV spectrometric instrumentation.

2.2. The SOLSPEC Spectrometer

The instrument has been described by Thuillier *et al.* (2009). SOLSPEC is made of three double-grating spectrometers named ultraviolet, visible, and infrared (UV, VIS, and IR), allowing measurements from 170 to 2900 nm. The spectral resolution is a weak function of the wavelength, which varies as shown in Table 1.

The wavelength sampling of the UV, VIS, and IR spectrometers is 0.4, 1, and 4 nm, respectively. SOLSPEC is also equipped by a set of quartz plates, which protect the spectrometers' optical diffuser from solar radiation below 160 nm and contaminant deposition. These plates are placed in front of the pre-slits, on two wheels with a hole, which permits measuring their transmission in space. Most of the time, the same quartz plate is used (# 1). About every two months, its transmission is measured by comparing two consecutive spectra with and without the quartz plate as well as the transmission of the second quartz plate,

Table 1 Spectral resolution ($\Delta\lambda$) of the UV, VIS, and IR spectrometers as a function of wavelength. Wavelengths and resolution are in μm and nm, respectively.

	UV				VIS				IR					
λ	0.18–0.24	0.26	0.30	0.34	0.30	0.45	0.60	0.75	0.85	0.70	1.2	1.7	2.3	2.9
$\Delta\lambda$	1.6	1.5	1.15	0.85	2.15	2	1.7	1.7	1.9	9.7	9.5	8.9	7.5	7

which is only measured by the same method every two months. This allows us to monitor the instrument ageing. The results are discussed in Section 2.4.

The instrument contains several light sources for use in space. One is a hollow cathode lamp, whose lines allow us to measure the relationship between wavelength and grating position. Furthermore, deuterium lamps and tungsten ribbon lamps provide information for the photometric scale of the three spectrometers. On 26 April 2009, the deuterium lamp power supply failed. Since then, we rely only on the tungsten ribbon and the hollow cathode lamp.

The optical entrance of each spectrometer consists of a pre-slit, a diffuser, and a slit. The diffuser allows us to reduce the effect of the CPD off-axis pointing. This effect consists in a change of recorded intensity of a source that has different positions in the instrument field-of-view. This effect can reach up to 5 %. Consequently, as the absolute calibration was performed for the centre of the field of view, it is necessary to know the Sun's position in the instrument field-of-view and the flat-field angular dependence. To achieve this, the optical axes of the three spectrometers are coaligned and a unique sun-sensor allows us to measure the Sun's position in the field of view. The flat-field dependence is measured in orbit by a special operation called criss-cross, which we describe in Section 2.3.

Absolute calibration measurements and calibration data processing are explained in Thuillier *et al.* (2009). The accuracy is a function of wavelength, but remains below 2 %, except at 3000 nm.

However, this uncertainty budget may increase because of the possible de-adjustment of some optical parts at launch, and the harsh space environment with particle precipitation on electronics, detectors, optics, and contamination by the outgassing from different equipments. The latter cause of ageing has been considered during the instrument design, and there is a very tight shutter that is closed when the instrument is turned off, in particular, during shuttle docking. In addition, the spectrometers' entrance diffusers remain warm to avoid contamination deposition.

Nevertheless, ageing does occur in space. Therefore two lamps with frequent and infrequent regimes are used. The amplitude of the infrequent lamp signal leads to a supplementary uncertainty of 1.4 %, which results in a total uncertainty of 3.4 %, *i.e.* below 3.5 %.

2.3. Operations in Orbit

The three instruments placed on the CPD observe the Sun up to 20 minutes *per* orbit. However, observations on an average of ten days *per* solar rotation are available, given the position of the ISS solar panels that power its equipment. The CPD also has the capability to scan the Sun in two orthogonal directions to measure the instruments' flat-field and the position of each instrument's optical axis with respect to the CPD axis of reference. Each solar measurement is followed by calibration measurements. When the Sun is not visible, the calibration data are recorded weekly.

2.3.1. SolACES

SolACES uses channel electron multipliers (CEMs) (http://Xw.sjuts.com/CEMModels_Standard.html), which are detectors working in the EUV. Because of the ageing of these detectors with respect to the accumulated count rates and managing the limited supply of the gases for the operation of the ionization chambers, the number of spectrometric recordings was steadily decreased with time. At the same time, the IC operations were increased to a degree so that for every day of operation, there is one recording either by the spectrometers or by the ionization chambers. Since the modelling of the IC currents allows derivating the EUV spectra, EUV spectral irradiance data are available for every day of the SOLAR mission operation. The very low leakage rates of the gas valves has allowed us to extend the SOLAR mission.

Although daily calibration of SolACES is not required, the ionization chambers are operated very frequently, even daily.

A special operation in space is the criss-cross manoeuvre: to check the alignment of the optical axis toward the Sun, the CPD is moved step-wise from +5 to -5 arcdegrees along the X and Y CPD axis. The strongest signals in the spectrometers and in the ionization chambers in each direction are used for the science measurements. Repeated criss-cross operations have allowed the verification of the alignment stability.

There are some other special characteristics of SolACES:

- The filters are used to determine the contribution of higher optical orders to correct the irradiance measurements. This is of particular interest for different levels of solar activity.
- The background caused by stray light can be quantified using the filters. Because it is below the statistical uncertainty of the count rates, a correction for the stray light background can be neglected.
- At the beginning of the mission the average count rates exceeded 10^6 , resulting in a statistical uncertainty better than 10^{-3} .

2.3.2. SOLSPEC

In orbit, the nominal operations depend on the periods when the Sun is visible or not (Sun or no-Sun visibility) of the SOLAR CPD. First light occurred on 5 April 2008. In the Sun-visibility window, SOLSPEC performs solar-irradiance measurements and internal intensity and wavelength calibrations. Since the beginning of Cycle 24, the Mg II (280 nm range) and Ca II (393 nm range) indices have been measured at high spectral sampling to monitor the development of the solar activity. In the no-Sun visibility window, only internal calibrations are run. During the solar minimum period, the solar spectrum was measured every two days. This sampling rate was increased as a function of the solar activity development.

To know in detail the behaviour and the ageing of SOLSPEC, special operations are scheduled to gather the following measurements:

- detector dark-current,
- instrument scattered light, transmission,
- flat-field of the three spectrometers by criss-cross manoeuvres,
- improvement of the signal-to-noise ratio in the spectral domain of weak instrument counting.

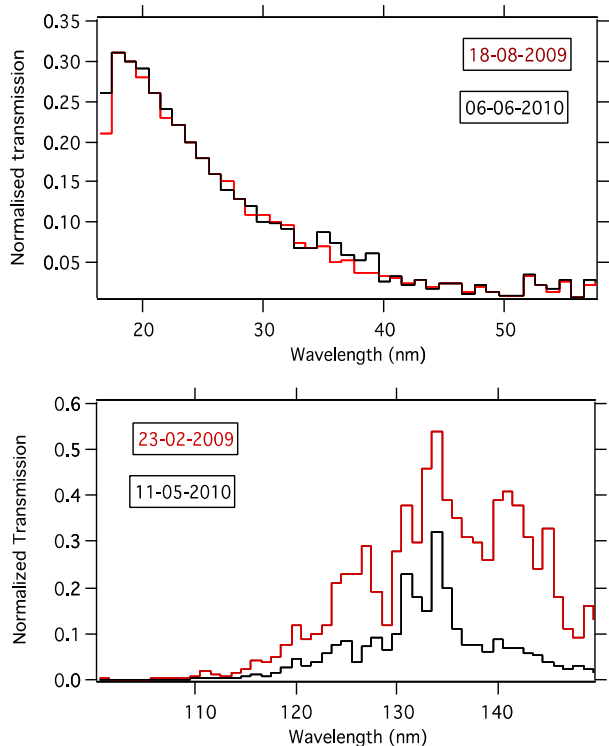
2.4. Calibration Results in Orbit

2.4.1. SolACES

The calibration is performed with a set of EUV filters that transmit spectral subranges such that the total EUV range of interest is covered. Because the efficiencies of the EUV components are changing with time, the transmission of each filter has to be determined repeatedly by direct measurements.

Figure 2 presents two typical cases: i) The transmission shown in Figure 2 (upper panel) is typical of the thin-film Al-C filters of different thicknesses, hence with different transmissions. The onboard calibration means allow us to determine the filter transmissions on 18 August 2009 and on 6 June 2010. The derived transmissions are still the same, with a smooth decrease from 17 nm to 50 nm as expected from the properties of the material used for the filters. A change of transmission is noticeable between 35 nm and 40 nm for the 6 June 2010 measurements when compared with the data from 18 August 2009. The explanation is the following: the transmission is measured by increasing the wavelength from 16 nm. The intense He II line at 30.4 nm generates a high count rate, but this is lower than 10^5 counts s^{-1} for the first date, because the solar activity is lower than during the second date. Consequently, the measured transmission for the first date presents the expected smooth decrease with wavelength. For the second date, the signal generated by the strong He II line induces a non-linearity and a perturbation of the channeltron, which is a property of this detector. Calibrating this effect allows correcting the data. In the upper panel of Figure 2, the raw data are shown (*i.e.* without correction).

Figure 2 Transmission of SolACES filters: aluminum-carbon (Al-C) filter (17–52 nm, upper panel) and the interference filter (115–145 nm, lower panel) after one year in orbit. We show with different colours the transmissions measured on different dates, which are indicated in the insets.



ii) To determine the photon fluxes in the spectral range from 110 nm to 150 nm (see Figure 2, lower panel), two sets of interference filters are used. These filters exhibit an unexpected individual behaviour by changing the transmission with wavelength. The transmission may decrease as well increase, as has been experienced for instance in the *San Marco Airglow-Solar Spectrometer Instrument* (Worden *et al.*, 1996). One filter set covers the range close to the Ly α emission, while the other set is centred around 135 nm including Ly α . The transmission change of one filter set out of the latter set is shown in Figure 2 (lower panel). The different spectral distributions of the two transmitted spectral intervals are evident and caused by the changing solar activity. For all filters in operation the transmissions are a smooth function of wavelength, except at the absorption boundaries of elements used in the filter manufacture.

2.4.2. SOLSPEC

All instruments have an angular photometric instrument dependence (flat-field) that consists of the following: when the source is placed at the instrument optical axis, it generates a signal with a given intensity, for example, 1. When the source is not at the optical axis, the same source generates a different signal that is generally lower, reaching 5 %, for example. This may affect the accuracy of the measurement:

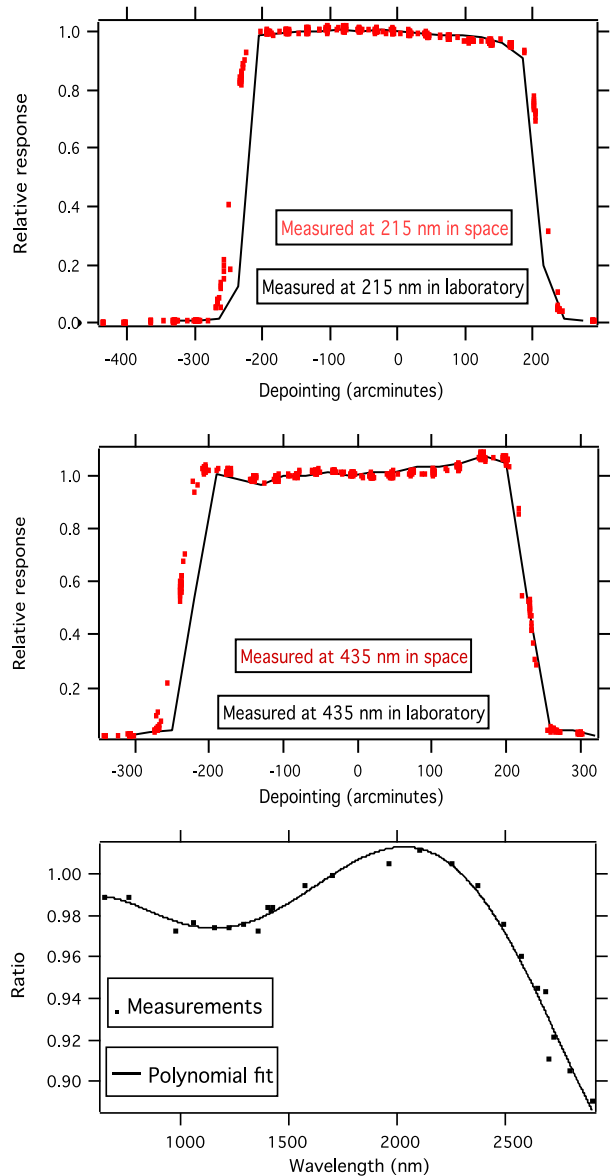
- on the ground the absolute calibration is achieved with the source aligned on the optical axis,
- in space this condition may not always be met (problem of pointing or post-launch misalignment),
- the flat-field is measured in the laboratory, but this is a difficult measurement especially in UV because of the scattered light and the geometry of the source beam and its intensity, which is much lower than that of the Sun. Therefore this is frequently performed in space using the Sun as source.

Consequently, we measured the instrument flat-field in space. Using the SOLSPEC sun-sensor and an appropriate motion of the CPD (criss-cross), the three spectrometers' fields-of-view (8 arcdegrees) were scanned at different wavelengths along two orthogonal directions. Figure 3 presents some examples. Figure 3 (upper panel) displays the SOLSPEC flat-field in UV measured orthogonally to the entrance slit. Figure 3 (middle panel) shows the SOLSPEC flat-field of the visible spectrometer measured along the entrance slit. For these spectrometers, the dependence on wavelength is within the accuracy of the measurements. For the IR spectrometer, however, a significant dependence on wavelength of the Sun's position within the field of view was measured, depending on whether the scan direction is along or orthogonal to the rectangular IR slit. Figure 3 (lower panel) shows the IR spectrometer flat-field measurements (dots) and their polynomial fit as a function of wavelength. The determination of the flat-field dependence on wavelength required a long sequence of measurements.

In orbit, an offset of about 1.5 arcdegree was initially found between the CPD axis and the SOLSPEC optical axis. The reason is a misalignment during the integration of SOLSPEC in the CPD. After adopting the offset pointing, which was compatible with the three instruments, the instrument flat-field was measured as a function of wavelength (Figure 3), showing the importance of the correction to be taken into account, especially in the IR domain (Figure 3, lower panel). Finally, thanks to the Sun sensor and because we know the flat-field, the effect of any residual off-axis pointing during the solar measurements can be corrected for.

An important aspect of the instrument performance is the ageing. Figure 4 shows the results for the UV, visible, and IR spectrometers. In the UV, Figure 4 (upper-left panel)

Figure 3 SOLSPEC spectrometer flat-field dependence in the UV (left panel) in the visible (middle panel) and in the IR (lower panel) (Bolsée, 2012). These data were obtained in May and June 2008.



shows the decrease measured by the Sun- and deuterium-lamp signals. This indicates how corrections can be made. About May 2009, a change of the ageing rate was observed (Figure 4, upper-left panel) and no explanation was found. This rate of change significantly decreased (Figure 4, upper-right panel plotted since 2010 to show the changed ageing rate). Figure 4 (upper-right panel) shows the ageing decreasing with wavelength. Figure 4 (middle-left panel) shows the near-UV part of the visible spectrometer signal generated by the Sun. An ageing is observed, while in the visible spectral domain, no ageing is detected (middle-right panel). Figure 4 (lower panel) shows the stability of the IR solar signal spectrometer, which stabilized by the end of 2008.

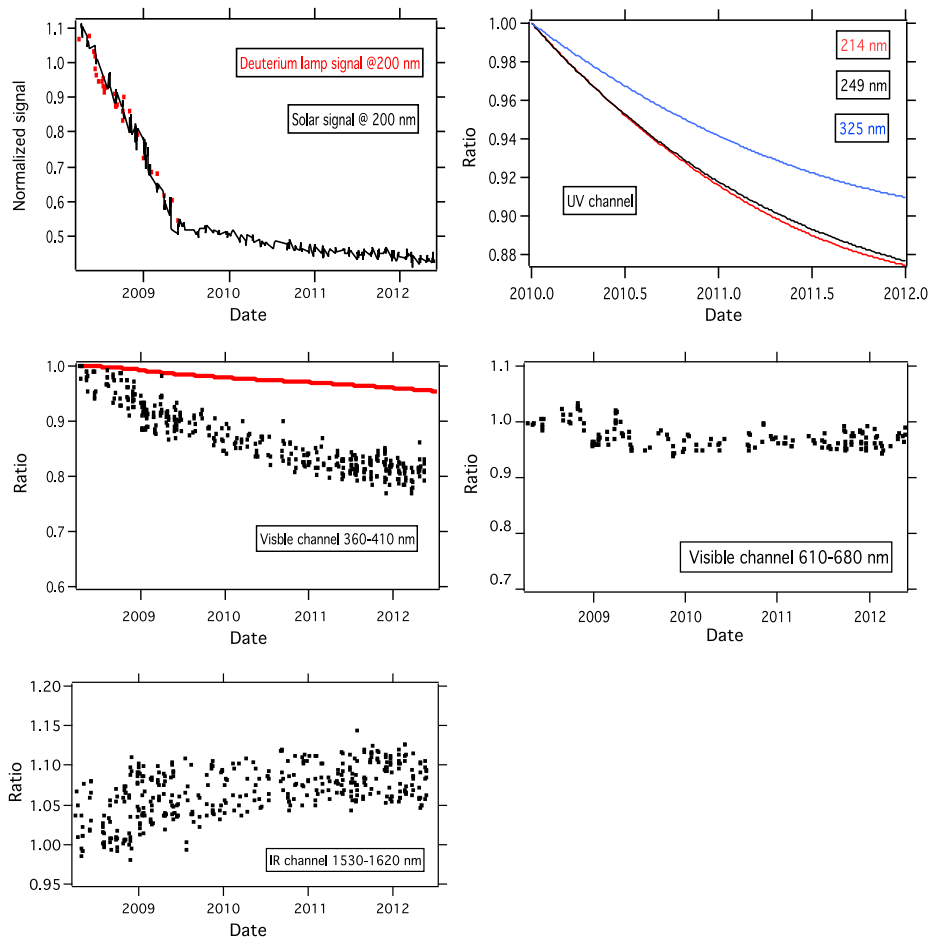


Figure 4 Ageing of the SOLSPEC UV spectrometer (upper panels). The upper-left panel shows a significant change in the instrument responsivity that appeared after the deuterium lamp power-supply failure (April 2009). The rate of change significantly decreased, as shown in the upper-right panel, which is plotted since 2010. Results for the visible spectrometer are shown in the middle-left and -right panels, the red line in the middle-left panel shows the ageing of the quartz mobile window. Results for the IR spectrometer are presented in the lower panel (Bolsée, 2012).

3. The Sun at Its Minimum Activity

3.1. The Composite Spectrum at Solar Minimum Activity

Very likely, the Sun was at its minimum activity around 2008–2009, as shown by, for example, with the F10.7 cm solar radio flux and sunspot number. Information from different sources allows us to specify the timing. A composite spectrum using the minimum SSI from SolACES and SOLSPEC will be built.

The SolACES data as displayed in Figure 5 (upper panel) show a minimum of the EUV irradiance on 21 August 2009. In Figure 5 (middle panel), the SORCE/SIM SSI at 215 nm shows a minimum around 26 June 2008. Furthermore, Figure 5 (lower panel) presents the

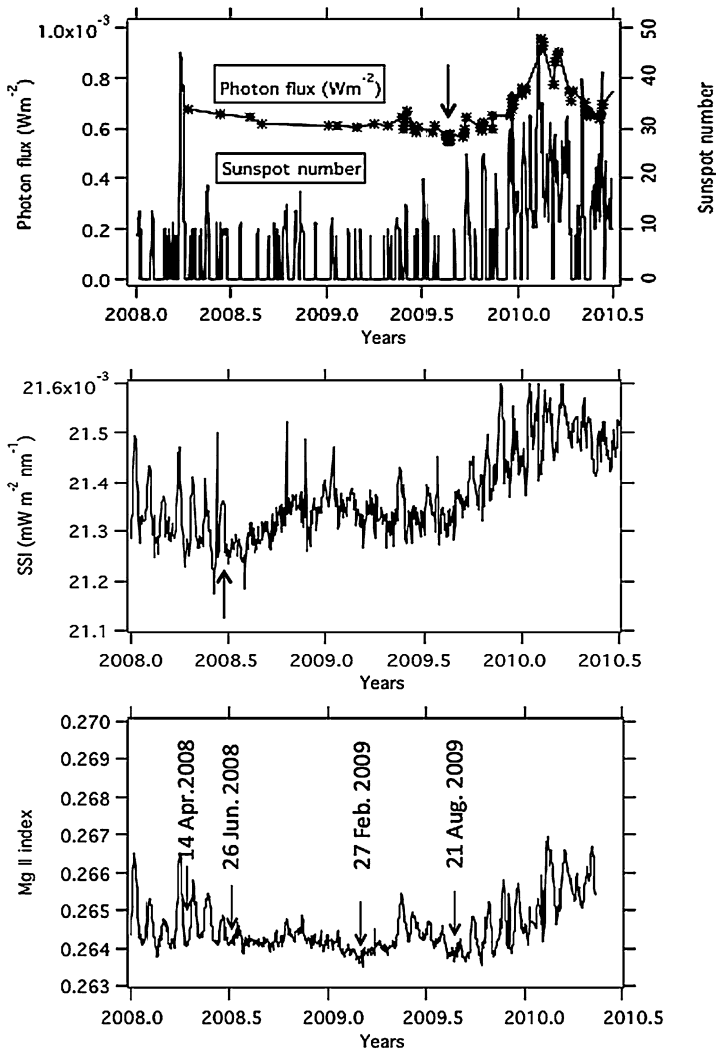


Figure 5 (Upper panel) SolACES photon flux (Wm^{-2}) integrated from 16 to 29 nm and sunspot number during the solar-minimum period between Solar Cycles 23 and 24 (Nikutowski *et al.*, 2011); the arrow shows the minimum EUV SSI that occurred on 21 August 2009. (Middle panel) SORCE-SIM data at 210 nm show a minimum located around 26 June 2008. (Lower panel) Mg II index variation as a function of time. The arrows point to the values on 14 April 2008, 26 June 2008, 27 February 2009, and 21 August 2009.

Mg II index as a function of time calculated by Viereck *et al.* (2004) based on the method developed by DeLand and Cebula (1998). A minimum occurs on 27 February 2009. The Mg II indices are 0.26411 on 26 June 2008, 0.16359 on 27 February 2009, and 0.26375 on 21 August 2009.

The Mg II indices are affected by an uncertainty that was found by Snow *et al.* (2005a) to be between 0.1 to 0.2 %, depending on the data set used to calculate it. Using a mean value of 0.15 %, the values mentioned above remain within their uncertainty limits. However, if the Mg II index is suitable to represent the UV SSI change, its variability is not precisely related

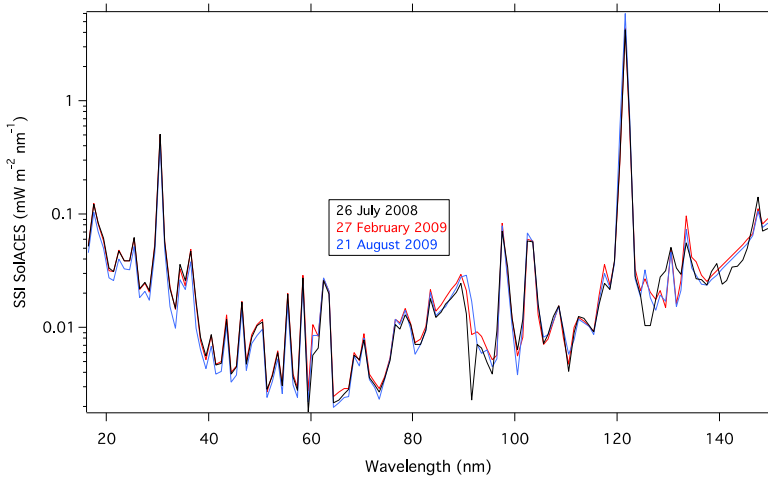


Figure 6 EUV SSI measured by SolACES for three dates: 26 July 2008 (black), 27 February 2009 (red), and 21 August 2009 (blue).

to the EUV domain variability. Therefore the EUV SSI for these three dates is compared in Figure 6. Taking into account that for these three dates the solar activity is close to minimum and that the effect of activity is stronger in the short-wavelength domain, the search of the minimum-activity SSI has to be made at short EUV wavelengths. For this, we calculated the ratio of the SSI on 26 June to that on 21 August and of that on 27 February to that on 21 August. Below 60 nm, these two ratios are 1.20, that is, 20 % above one, which is not explained by the combined uncertainty of each data set (10 %).

Consequently, this suggests that the SSI minimum in a given wavelength range depends on the date; the minimum occurs later in an emission which originates in the upper chromosphere than when it comes from a lower altitude.

In line with this question, White *et al.* (2011) have determined the date of the solar minimum using the TSI, the F10.7 cm radio flux, and the Mg II index. Three distinct minima were found on 15 October 2008, 11 November 2008, and 2 December 2008, respectively. These dates were obtained after a polynomial smoothing of the corresponding data over eight solar rotations. Consequently, they are approximate, and not in phase. The smoothing over eight months and the nature of the data (TSI, F10.7) make a detailed comparison with our work difficult because we used a different method and data to determine the dates of the minimum.

To build the SSI at solar minimum from the available ISS measurements, the most representative data have to be selected. For SOLSPEC and SolACES, various constraints led us to choose the date of solar minimum-activity taking into account the different technical operations onboard the ISS, the flat-field measurements, the pointing toward the Sun, and to be as close as possible to the whole heliospheric interval (WHI: Woods *et al.*, 2009) time-frame to perform a simple comparison between the two datasets. This condition associated with first light, which occurred on 5 April 2008, has allowed us to avoid correcting for ageing, which in any case would be possible by using of the onboard set of lamps. We selected the following days: 8 April and 2, 4, and 6 May 2008 for SOLSPEC UV to IR data, which allow for an appropriate signal-to-noise ratio and are close to first light, and 21 August for SolACES in the EUV.

Table 2 Dates, sunspot number (SSN), F10.7 cm radio flux, and Mg II index for the intervals used in this article. For data covering several days, the mean values of the SSN, Mg II index, and F10.7 solar radio flux are shown.

	ATLAS 3	WHI	SOLSPEC	SOLSTICE	SOLACES	EVE
Date	10 Nov. 1994	10, 16 Apr. 2008	5, 8 Apr., 2, 4, 5 May 2008	5 Apr. 2008	21 Aug. 2009	14 Apr. 2008
SSN	18	<2>	<3>	0.0	0.0	7
F10.7	80.	<68.9>	<68>	71.3	67.0	68.9
Mg II index	0.26747	<0.26416>	<0.26433>	0.26465	0.26375	0.26416

The spectral domains covered by the ISS spectrometers are 16 nm to 149.5 nm by SolACES and 170 nm to 2900 nm by SOLSPEC. To fill the gap, we used data obtained with SORCE/SOLSTICE from 149.5 to 170 nm on 5 April as follows: between 139.5 and 149.5 nm, we used SolACES and SOLSTICE with a linear transition between the two datasets (100 % of SolACES data and 0 % of SOLSTICE data at 139.5 nm; and 0 % of SolACES and 100 % of SOLSTICE at 149.5 nm). We proceeded similarly between 166.5 and 176 nm.

With the data obtained from the ISS instruments and the ATLAS 3 spectrum, we built two composite spectra:

- SOLAR 1 uses measurements from SolACES, SOLSTICE and SOLSPEC as explained above, except between 1100 to 2400 nm where the ATLAS 3 IR part was used.
- SOLAR 2 used only measurements from SolACES, SOLSTICE and SOLSPEC.

This is justified in Section 3.3.3. It is important to remember that the only difference between SOLAR 1 and SOLAR 2 is in the IR.

Dates, Mg II index, sunspot number (SSN), and F10.7 cm radio flux are given in Table 2, which shows that the three data sets are selected in very quiet solar conditions with a sunspot number not larger than 3 and an F10.7 cm radio flux ranging between 67 to 71 units.

3.2. Photometric Properties of the SOLAR 1 and 2 Composite Spectra

The different photometric properties of SOLAR 1 and 2 spectra were compared with other measured and theoretical spectra.

3.2.1. Measured Spectra

We compared the following spectra:

- the WHI spectrum (Woods *et al.*, 2009) with an accuracy wavelength-dependence of 10 to 15 % in the EUV and 2 to 5 % in the UV
- data from the SDO/EVE prototype, obtained during a rocket flight on 14 April 2008, in preparation for the SDO mission
- the spectrum obtained during the mission *Atmospheric Laboratory for Applications and Science* (ATLAS) 3 (Thuillier *et al.*, 2004) available from 0.5 to 2400 nm, which corresponds to a low-activity period, and
- the SCIAMACHY data (see Section 1.1).

3.2.2. Theoretical Spectra

Different physical processes contribute to the UV, visible, and infrared parts of the solar spectrum. The main source of the continuum opacity in the far UV (below approximately 160 nm) is photoionization of heavy elements, which means that most of the photons are generated by recombination processes in the photosphere. On top of the continuum there are several strong emission lines (the most prominent line is Ly α), which are formed in the chromosphere. Starting from approximately 160 nm, the opacity is dominated by the immense number of unresolved weak spectral lines, which are absent from the existing line lists (see *e.g.* Busa *et al.*, 2001; Short and Hauschildt, 2009). To take this into account, Shapiro *et al.* (2010) introduced additional UV opacity in COSI. Starting from approximately 320 nm, the main sources of the opacity are bound-free (up to approximately 1650 nm, which corresponds to the negative hydrogen ion H^- ionization energy) and free-free transitions in H^- . The visible spectrum is superposed with a large amount of absorption spectral lines (*e.g.* Ca II or neutral hydrogen lines) and molecular system (*e.g.* CH, NH, and OH bands at 310–340 nm, the CN violet system at 375–390 nm, and the CH G band at 410–450 nm). The H^- opacity has a local maximum at about 850 nm, then it decreases up to approximately 1650 nm, and then increases again (*cf.* Mihalas, 1978).

In this section we present two synthetic solar spectra calculated with COSI (Haberreiter, Schmutz, and Hubeny, 2008; Shapiro *et al.*, 2010), and the Solar Irradiance Physical Modelling (SRPM) system (Fontenla *et al.*, 2011).

COSI simultaneously solves the equations of the statistical equilibrium and radiative transfer, assuming a one-dimension (1D) spherically symmetric geometry. The spectra presented in this article were compared with the spectrum of the quiet Sun calculated with COSI. The temperature and density profiles were taken from Model C of Fontenla *et al.* (1999). In principle, COSI can be potentially used to calculate the spectrum from the EUV to radio waves. The most recent paper with a COSI description (Shapiro *et al.*, 2010) presented calculations that only started from 125 nm. In the 125–160 nm spectral domain, COSI misses several important emission lines (see Shapiro *et al.*, 2010), therefore we began the comparison at 160 nm.

An agreement between SRPM and ATLAS 3 was found previously (Fontenla *et al.*, 2006). Therefore we extended this comparison between the new version of the SRPM code (Fontenla *et al.*, 2011) and the new dataset provided by SOLAR 1 and 2.

Version 11 of SRPM calculates the solar irradiance by weighting the spectra of seven atmospheric components that correspond to the main features at the solar disc observed with ~ 2 arcsec resolution (Fontenla *et al.*, 2009, 2011). These spectra are calculated employing semi-empirical atmospheric models and a non-local thermodynamic equilibrium (NLTE) radiative transfer code, the development of which started almost two decades ago (see Fontenla *et al.*, 1999, and references therein). Because the spectra depend on the heliocentric angle, they are calculated for ten disc positions. The weighting coefficients are computed employing images obtained with the *Precision Solar Photometric Telescope* (PSPT). For the comparison presented here, we used the spectrum that was downloaded from http://www.digidyna.com/Results2010/spectra/irradiance/daysloresFitsfmt/index_spectra_irradiance_daysloresFitsfmt.html. Fontenla *et al.* (2011) calculated it by mixing the spectra of A + B (quiet-Sun inter-network), D (quiet-Sun network lane), F (enhanced network), and H (plage) components in different percentages (80 % (A + B) + 18.9 % D + 1.1 % F + 0.0064 % H). This spectrum is calculated for low solar activity conditions (15 September 2008).

3.3. Comparison with Measured and Theoretical Spectra

To determine the photometric differences between a set of spectra, we integrated the SSI in several wavelength domains and calculated their ratio, which provided differences in percent. The optical instruments have no constant wavelength signal-to-noise ratios because the components they use have properties (transmission, grating efficiency, detector efficiency) that all depend differently on the wavelength. Another contribution originates from the calibration source (blackbody, Synchrotron Ultraviolet Radiation Facility (SURF) radiation, lamps). A final concern is the SSI, which presents significant changes with wavelength. Consequently, the signal-to-noise ratio varies with wavelength, and this variation is instrument dependent. Therefore we used several spectra selected under nearly the same condition of solar activity for the comparison. Consequently, the ratio of two spectra calculated in different spectral domains oscillates around unity. However, if the domain of integration is large, the ratio generally comes closer to unity.

Furthermore, to show the photometric difference between two spectra, we calculated the SSI in some wavelength intervals and their ratio. The noise and the wavelength scale difference contain different spectrometer point-spread functions (psf) in certain spectra, and spectral sampling may generate a spurious irradiance ratio.

3.3.1. Comparison in the Spectral Domain below 200 nm

Figure 7 displays all datasets listed in Section 3.2 that are below 110 nm. There is an overall agreement; but there are differences varying with wavelength. The upper and lower panels show that SolACES presents a lower SSI than all other spectra. ATLAS 3 presents the highest SSI for the strong lines, as expected because it was obtained at higher solar activity. We also note that the WHI continuum remains lower than all other spectra.

The lower panel of Figure 7 shows that the SolACES SSI appears very close to the WHI above 35 nm, and is lower than WHI at 18 nm.

To estimate the percentages of the photometric differences between these spectra, in each spectral domain, the integrated SSI was calculated for each spectrum, then ratios were computed, which are shown in Table 3. The percentage of the photometric difference was compared with the combined uncertainty of the two spectra involved in this comparison. Given that SolACES and the other spectra have an accuracy of about 10 and 25 %, respectively, the combined uncertainty is 27 % at one σ . Two spectra are different when their ratio is beyond the range ± 27 % at one σ .

For wavelength ranges below Ly α , we can see from Table 3 that:

- The closest agreement is achieved between WHI and SOLAR 1 in the range 16 to 120 nm. Nevertheless, within that domain there are variations that we show below.
- The WHI/ATLAS 3 ratio presents two extreme values at 1.33 and 0.69 in the EUV, which decrease towards the UV, however. These ratios are compatible with the combined uncertainty of each data set (see above). We also note that the solar activity for the WHI was lower than during the ATLAS 3 period (Table 2).
- In the range 96–100 nm, SolACES presents the largest difference with respect to the three other spectra.
- As a general rule, above Ly α , the ATLAS 3, SOLAR 1, and WHI differences are smaller than their values in the EUV range. In particular, the absolute calibration becomes more precise when the solar variability is weaker, which provides a closer SSI.

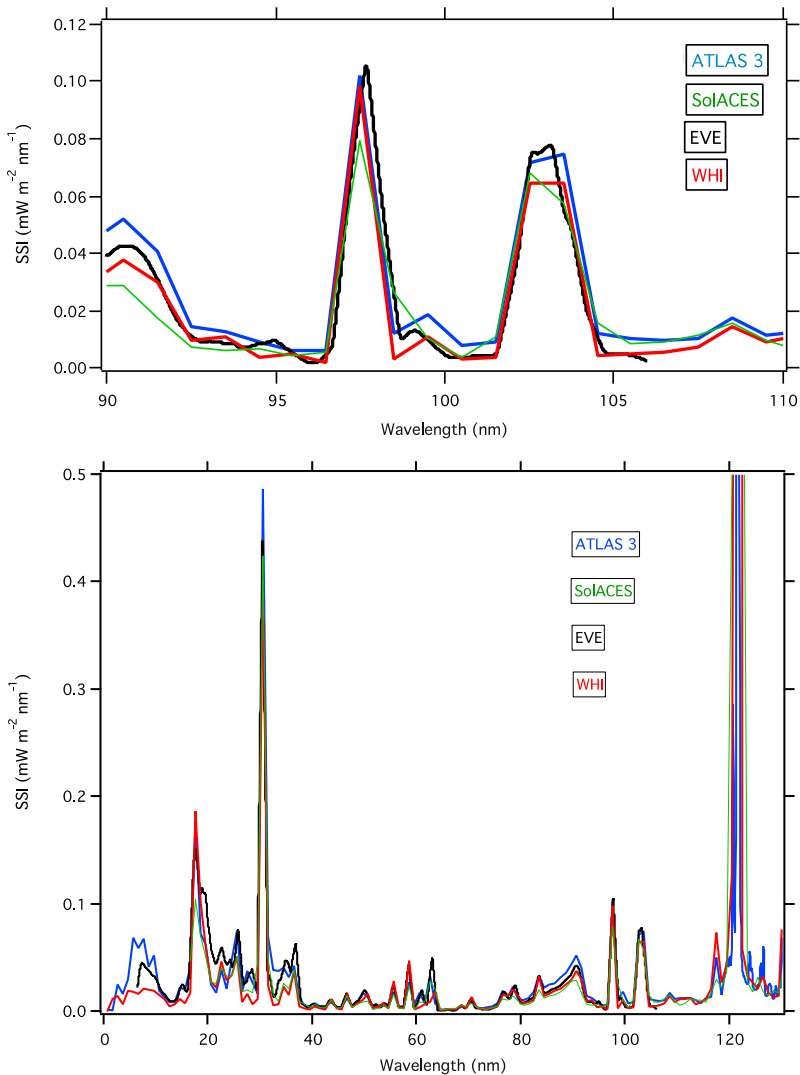


Figure 7 Comparison between the SSI measured by the ATLAS 3, WHI, SolACES, and the EVE rocket flight on 14 April 2008. The resolution of the spectra is 0.1 nm for WHI and EVE and 0.2 nm for ATLAS 3. For SolACES, it is 0.3 nm below 65 nm and 0.4 nm between 65 and 100 nm. Upper and lower panels show the spectral ranges 0–110 nm and 90–110 nm, respectively. The colour of the curves is the same as the name of the corresponding instrument or campaign in the insets.

– To compare COSI with ATLAS 3 and WHI, we used the ratios given in Table 3. The WHI/SOL and COSI/SOL ratios are almost equal; this indicates that COSI and WHI values differ within 2%. Similarly, considering the ratio WHI/A3 shows that COSI is closer to WHI than to ATLAS 3. This is expected, considering that the solar activity was different.

In the ranges below 150 nm, it must be taken into account that the SOLAR/SOLSTICE data were calibrated at the SURF III of the National Institute of Standards and Technology

Table 3 Ratio of SSI in specific wavelength domains as indicated in the first column between ATLAS 3 (A3), WHI, COSI, and SOLAR 1 below 200 nm (see third, fourth, fifth, and sixth columns). The second column indicates the main spectral features (lines or continuum) in the wavelength range. Empty lines indicate that the data are not available for the calculation.

$\Delta\lambda$ [nm]	Lines/continuum	A3/SOL	WHI/SOL	COSI/SOL	WHI/A3
17–120	See below	1.06	0.95		0.90
15–25	Fe XVII, O VIII, Cr XV, Ca XIV, ...				1.05
28–35	He II, Fe XVI	1.09	0.75		0.69
55–65	He I, O VI	0.95	1.26		1.33
96–100	C III, Ly γ , N III	1.48	1.28		0.86
101–105	Ly β , O VI, C III	1.05	0.87		0.83
121–122	Ly α	1.42	1.38		0.96
166–180	continuum	1.06	0.97	0.97	0.92
120–200	continuum, O II, C II, Si IV, C IV, Si II	1.06	1.00	0.95	0.94
180–220	continuum, Si II, Al edge	1.03	0.95	0.97	0.92
170–207	continuum, Si II, Al edge	1.04	0.98	1.00	0.94
207–300	deep Fraunhofer lines	1.04	0.97	0.98	0.94

(NIST) facility using quiet blue stars to track relative changes in the instrument (Snow *et al.*, 2005b), while SolACES measurements were calibrated in the absolute scale using ionization chambers. These two techniques have different characteristics. This comparison shows that they agree with a mean difference of 20 %. This represents a significant improvement with respect to datasets gathered in the 1980s.

3.3.2. Comparison in the Spectral Domain 200–850 nm

Figure 8 displays six spectra. They each have a different sampling, psf, spectral resolution, and most likely small (0.1 nm) wavelength-scale differences. To point out photometric differences instead of spectral differences, each spectrum was averaged over the five nm running mean with one nm step. The consistency between the original spectra and the resulting smoothing was carefully determined, in particular the SRPM dataset provided on its website (Section 3.2), which is a very high resolution spectrum (0.02 nm below 1000.4 nm and 0.1 nm above).

Figure 8 displays the measured spectra of ATLAS 3, SCIAMACHY, SOLAR 1, and WHI and the theoretical spectra derived from COSI and SRPM data from 150 to 850 nm. Figure 8 (upper panel) shows the agreement between the measured spectra and COSI, but a difference between SCIAMACHY and ATLAS 3 with respect to COSI, SOLAR 1, and WHI is noteworthy at 270 nm. The SRPM spectrum shows some differences with respect to the others. Figure 8 (middle panel) displays the measured and theoretical spectra up to 400 nm. ATLAS 3, COSI, SCIAMACHY, SOLAR 1 and WHI remain in close agreement, but there is a discrepancy with COSI around 350 nm, which has previously been identified (Thuillier *et al.*, 2012). Finally, Figure 8 (lower panel) shows an overall agreement between ATLAS 3, COSI, SCIAMACHY, SOLAR 1, and WHY. Nevertheless, the WHY spectrum presents a systematically lower irradiance measured above 600 nm than the other three. The SSI from SRPM is higher than all other spectra between 460 and 600 nm, while above this it joins the ATLAS 3, COSI, SCIAMACHY, and SOLAR 1 spectra.

To clarify the differences between these spectra, their SSIs were calculated (as in Section 3.3.1) in several spectral ranges, and their ratios are shown in Table 4.

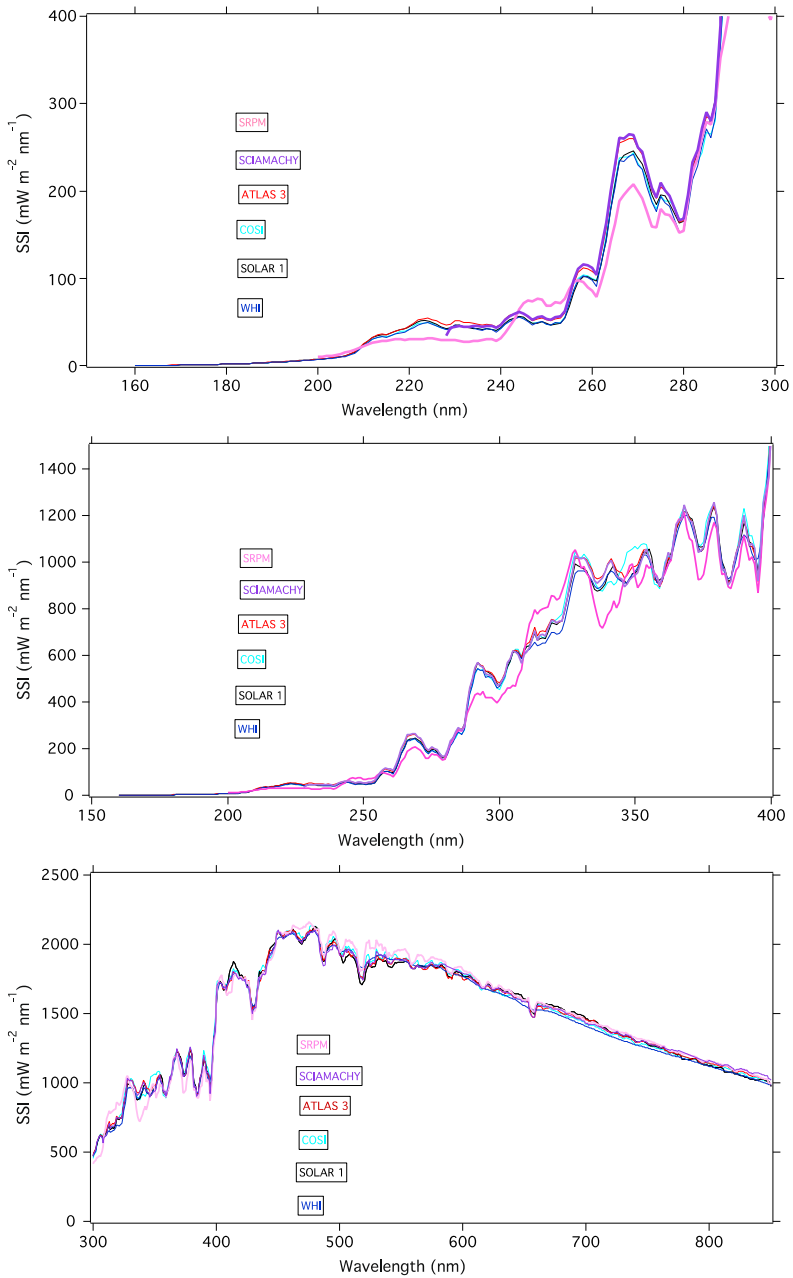


Figure 8 Comparison between the solar spectral irradiance measured by ATLAS 3, SCIAMACHY, SOLAR 1, and WHI and the COSI and SRPM theoretical spectra. The upper, middle, and lower panels show the spectral range 150 to 300 nm, 150 to 400 nm, and 350 to 850 nm, respectively. Differences are easily detectable especially below 400 nm.

Table 4 Ratio of power *per* spectral range (first column) for SRPM, ATLAS 3 (A3), WHI, and COSI, to SOLAR 1 (SOL), WHI to ATLAS 3, and COSI, and SRPM to COSI in the range 200–800 nm.

$\Delta\lambda$ [nm]	SRPM/SOL	COSI/SOL	A3/SOL	WHI/SOL	WHI/A3	WHI/COSI	SRPM/COSI
210–350	0.96	1.01	1.03	0.98	0.95	0.96	0.95
350–500	0.99	1.00	1.00	0.99	0.99	0.98	0.98
350–850	1.01	1.00	1.00	0.99	0.99	0.99	1.01
220–260	0.95	1.00	1.09	0.98	0.90	0.99	0.95
260–300	0.85	0.97	1.02	0.97	0.94	0.99	0.87
300–340	1.01	1.02	1.03	0.98	0.95	0.96	0.99
340–370	0.96	1.02	1.00	0.99	0.98	0.97	0.95
350–425	0.97	1.00	0.99	0.99	0.99	0.98	0.96
425–500	1.00	1.00	1.00	0.99	0.99	0.99	1.00
500–575	1.05	1.02	1.01	1.02	1.01	1.00	1.02
575–650	1.01	0.99	0.99	0.99	0.99	0.99	1.01
650–725	1.00	0.98	0.99	0.97	0.98	0.99	1.02
725–800	1.02	0.99	1.00	0.98	0.98	0.99	1.02

The ratios WHI/SOL and WHI/COSI are within an interval of 0.97 to 1.02. Given that the measured spectra have an accuracy of 3 %, these three spectra agree considering their specific uncertainties. A3/SOL also presents a ratio close to unity, except in the domain 220–260 nm. This difference is consequently also found in the ratio WHI/A3. For large spectral intervals such as 350–850 nm, the five spectra have differences of the order of 1 %.

The agreement between COSI and SOLAR 1 remains at around 3 % or better, keeping in mind that the experimental spectra have an absolute uncertainty of about 3 % (wavelength dependent), while the uncertainties of the theoretical spectra (COSI and SRPM) are more difficult to estimate. In the range 300–340 nm (see Figure 8, middle panel), the COSI SSI is higher by 2 % than the three other spectra in the domain 300–340 nm. The main reason for this difference is the inaccuracy in the molecular line lists, that is, the solar spectrum at these wavelengths contains a few molecular bands (CH, NH, and OH), whose positions and oscillator strengths are not yet accurately known and taken into account in COSI.

The COSI calculations agree better with the WHI spectrum than with ATLAS 3 in the domain 240–340 nm (Table 4 and Figure 8, upper panel) where the COSI calculations basically coincide with the WHI spectrum. However, this cannot be considered as an independent proof, because Shapiro *et al.* (2010) adjusted the additional UV opacity in the 160–320 nm spectral region, using SORCE/SOLSTICE spectrum averaged over one week (21 April 2008–28 April 2008). Furthermore, the solar activity corresponding to the ATLAS 3 period is higher than the solar activity for the SOLAR 1 spectrum (Table 3). Shapiro *et al.* (2013) showed that the centre-to-limb variations of the solar brightness deduced from the *Large Yield RAdiometer* (LYRA) placed onboard the *PROject for OnBoard Autonomy 2* (PROBA2) satellite measurements provide an independent test of the additional UV opacity and agree well with the SORCE/SOLSTICE measurements. The difference between SRPM and the other spectra can be seen with its ratio to COSI. This ratio is 0.87 between 260 and 300 nm, as also shown in Figure 8 (upper panel). We are not able to explain the origin of these differences.

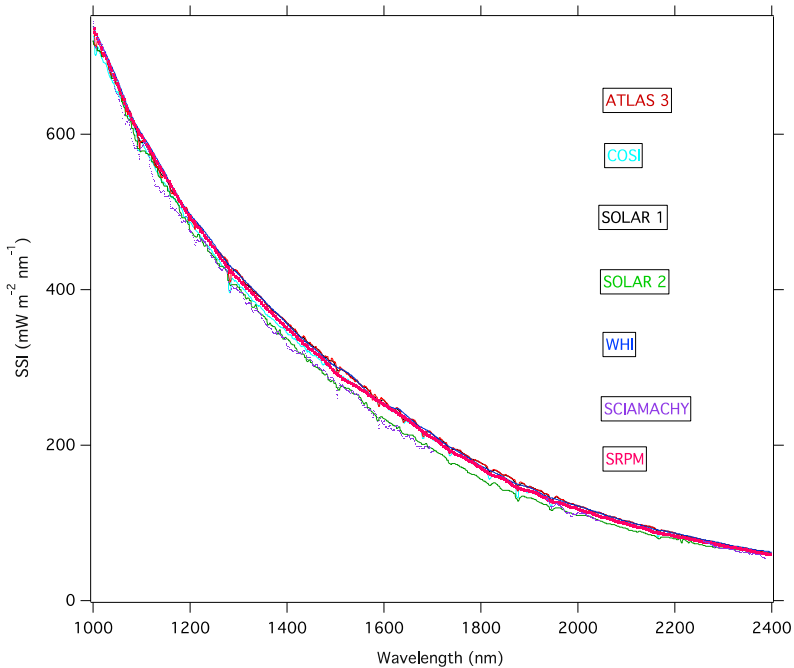


Figure 9 Comparison in the IR domain between the SSI measured by ATLAS 3, SOLAR 1, SOLAR 2, SCIAMACHY, and WHI and the prediction by the COSI and SRPM models. We recall that the SOLAR 1 and WHI spectra (both using SORCE/SIM) were adjusted to match ATLAS 3 in the IR.

3.3.3. Comparison in the Spectral Domain above 850 nm

Figure 9 compares the IR solar spectra above 1000 nm provided by ATLAS 3 and SOLAR 2. SOLAR 2 appears just below ATLAS 3 by 10 % at 1700 nm, which is incompatible with the accuracy of these two spectra as well as with a possible solar activity effect. An exhaustive investigation of possible causes was carried out to explain this discrepancy

- non-linearity of the IR electronics,
- diaphragm diameter,
- flat-field,
- dark current,
- IR detection linearity,
- during ground calibration using the blackbody source,
 - absorption by water vapour,
 - distance between source to the entrance pupil,
 - blackbody-source temperature drift,
- linearity in the signal digitization.

No explanation has been found yet. Therefore we built the two composites SOLAR 1 and SOLAR 2 (see Section 3.1), whose difference is between 1100 to 2400 nm where the ATLAS 3 IR part is used in SOLAR 1.

This choice was based on the agreement between the solar-atmosphere model (Fontenla *et al.*, 2006) and ATLAS 3, which shows a brightness-temperature difference between the

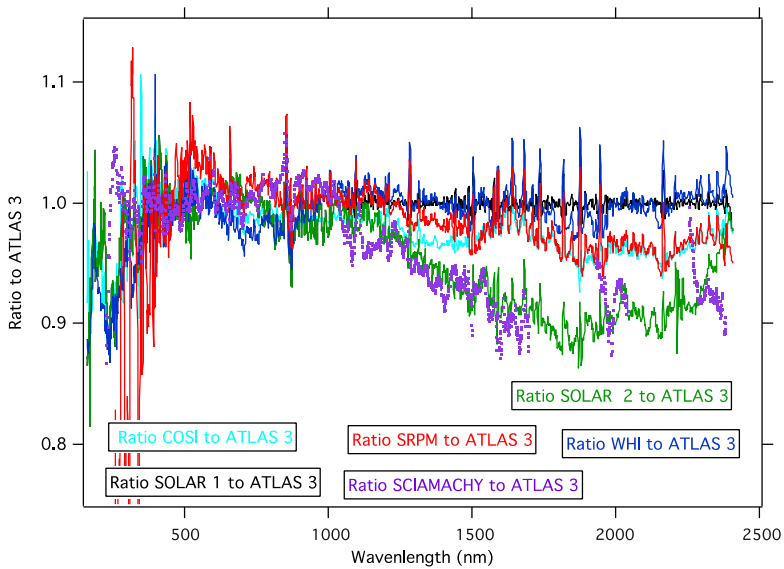


Figure 10 Ratio to ATLAS 3 of the SOLAR 1 and 2 composites, COSI, SRPM, SCIAMACHY, and WHI from 150 to 2400 nm. The main differences are in the IR. We recall that the SOLAR 1 and WHI spectra (using SORCE/SIM) were adjusted to match ATLAS 3 in the IR.

derived temperature and the modelled one of 150 K at 1600 nm that is lower at other wavelengths.

Because we were unable to determine the origin of the difference between SOLAR 2 and ATLAS 3 (see above), we used the SCIAMACHY spectrum to investigate this question. The spectra used in Section 3.2.2, and employed in Figures 10, 11, and 12 were smoothed by a running mean of five nm below 2400 nm and 20 nm above 2400 nm.

To emphasize the differences between the spectra, we calculated the ratio between each one and the same spectrum, which is ATLAS 3. These ratios are shown in Figure 10. As expected, WHI, ATLAS 3, and SOLAR 1 agree. The SRPM and COSI ratios to ATLAS 3 are close together (2 % at 1300 nm), and just around 3 to 4 % below unity in the IR domain. SCIAMACHY and SOLAR 2 are close until 1700 nm, and their agreement is slightly poorer in the two narrow spectral windows near 1.9 μm and 2.4 μm . However, both reach a 10 % difference at 1700 nm.

To be more precise in terms of agreement/disagreement between these spectra, the differences between spectra are shown by calculating the power (Wm^{-2}) in some specific domains and their ratio (*e.g.* WHI/ATLAS 3). The SCIAMACHY spectrum has many small data gaps, which prevent determining its photometric properties with respect to the other spectra because of the inaccuracy of the integration induced by the gaps. Therefore we did not calculate the corresponding ratios. Table 5 displays the ratios between spectra.

We note the following:

- ATLAS 3 and SOLAR 1 agree *per construction*. WHI also agrees with ATLAS 3 because its IR data were used in WHI (Harder *et al.*, 2010).
- SOLAR 2 presents its largest difference with respect to ATLAS 3 at around 2000 nm. However, when integrating from 1000 to 2400 nm, the difference decreases to 5 %, as expected.

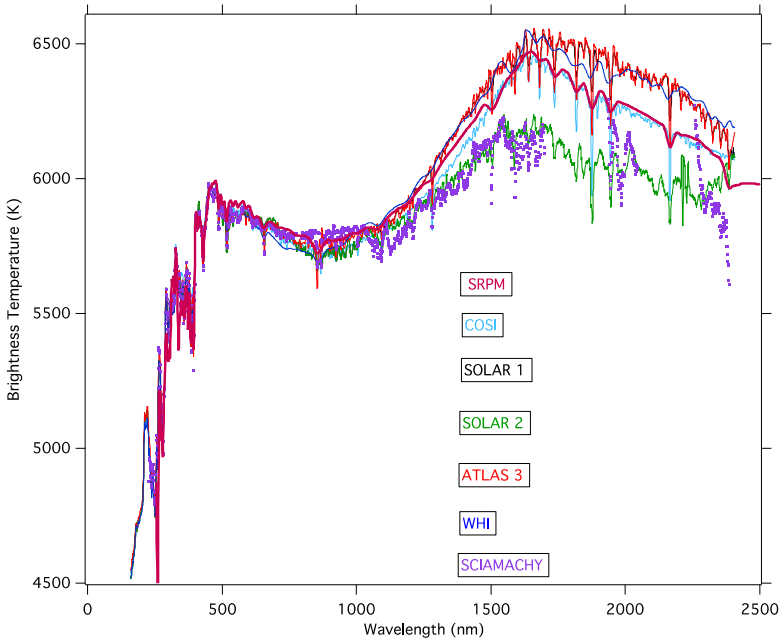


Figure 11 Calculated brightness-temperatures as a function of wavelength for all experimental spectra and the COSI and SRPM theoretical models from 200 to 2400 nm. We recall that the SOLAR 1 and WHI spectra (using SORCE/SIM) were adjusted to match ATLAS 3 in the IR. Because SOLAR 1 and ATLAS 3 are identical in the IR, the black curve (SOLAR 1) is not visible.

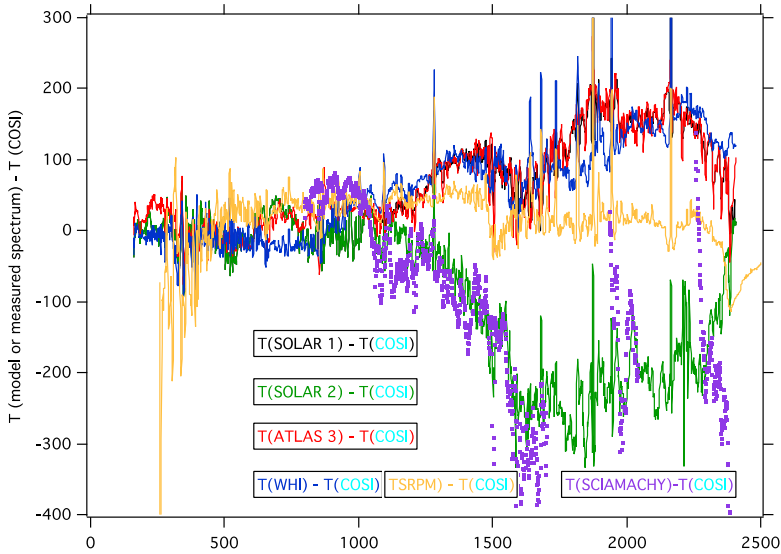


Figure 12 Difference in calculated temperatures as a function of wavelength for all experimental spectra and the COSI theoretical model from 200 to 2400 nm. We recall that the SOLAR 1 and WHI spectra (using SORCE/SIM) were adjusted to match ATLAS 3 in the IR. Because SOLAR 1 and ATLAS 3 are identical in the IR, the black curve (SOLAR 1) is not visible.

Table 5 Ratio *per* spectral range for SRPM, COSI, WHI, SOLAR 1 (SOL1), and SOLAR 2 (SOL2) to ATLAS 3 (A3) in the range 210 to 2400 nm, and COSI and SRPM to SOLAR 2 in the range 210–2900. Empty lines indicate that the data are not available for the calculation. SOLAR 1 and ATLAS 3 are identical between 1100 and 2400 nm.

$\Delta(\lambda)$	SRPM/A3	COSI/A3	WHI/A3	SOL1/A3	SOL2/A3	COSI/SOL2	SRPM/SOL2
210–2400	1.00	0.99	0.99	0.99	0.98	1.01	1.02
1000–2000	0.99	0.98	1.00	1.00	0.95	1.03	1.04
1000–1761	0.99	0.98	1.00	1.00	0.96	1.02	1.03
1000–2400	0.99	0.98	1.00	1.00	0.95	1.03	1.04
2100–2200	0.96	0.95	1.00	1.00	0.90	1.06	1.06
2400–2900						1.05	1.04

- In the domain 210–2400 nm COSI, WHI, and SOLAR 1 have nearly the same irradiance; this is also true in the domain 1000–2000 nm.
- The COSI to ATLAS 3 ratio remains close to unity (around 2 %) up to about 1800 nm, then it decreases to 5 %. In the interval 2400–2900 nm, COSI and SOLAR 2 agree to within 5 %.
- The SRPM to ATLAS 3 and COSI to ATLAS 3 ratios remain close to unity (around 1 to 2 %), except in the interval 2100–2200 nm.
- SRPM and COSI behave similarly when comparing their predictions with SOLAR 2 because these two models agree.

The absolute values of the irradiance in each domain allow us to clearly see the contribution of particular spectral bands to the TSI. While the main contribution to the TSI (> 97 % according to all measured and COSI spectra) originates from the range 210–2400 nm, the far-infrared contribution (2400–2900 nm) cannot be dismissed, because it is responsible for approximately 1.5 % of the TSI.

3.4. Derived Brightness Temperature from the Solar Spectra

Using a logarithmic scale above 800 nm to represent the solar spectra used in this article, the variations of the SSIs are quasi-linear as a function of wavelength. Thus, each spectrum allows us to calculate the solar brightness-temperature as a function of wavelength (Figure 11). However, this calculation emphasizes the presence of noise.

The brightness-temperature has a prominent maximum around 1650 nm (Figure 11). It corresponds to the minimum of the H^- opacity (see above). The photons at this wavelength come from the deepest layers of the photosphere and, as the temperature increases inward, they correspond to the highest effective temperature. Above 1650 nm, the H^- opacity starts to increase and the formation height of the photons shifts to higher and cooler regions so that the brightness temperature decreases.

In the infrared, the solar irradiance depends on the brightness-temperature in an approximately linear way (as the Planck function can be approximated by the Rayleigh–Jeans law). Thus, even small deviations between different spectra result in large brightness-temperature differences. By studying them, one can very carefully compare the spectra (*e.g.* the deviations are hardly visible in Figure 11, but are very prominent in Figure 12 with respect to COSI). Figures 11 and 12 show the brightness temperature derived from all spectra, in particular from the SCIAMACHY spectrum. Up to 1100 nm, its derived temperature remains

Table 6 Power (Wm^{-2}) in the spectral domain 1000–1761 nm for each spectrum. Dataset names are abbreviated as in Table 5.

SRPM	COSI	A3	WHI	SOL1	SOL2	SCI
299.4	294.9	300.9	302.7	299.8	288.6	286.6

consistent with the others. Above this, the temperature remains between the SOLAR 2 and SOLAR 1 derived brightness-temperature despite the noise.

We note the agreement of the retrieved brightness-temperatures from the ATLAS 3, WHI, SOLAR 1 (*per* construction), and COSI and SRPM temperatures. In particular, we note the agreement of the predicted maximum temperature also obtained with ATLAS 3 spectrum at the same wavelength (~ 1650 nm). However, these two groups present a difference of about 50 K up to 1100 nm. This difference reaches 150 K at 2000 nm. The SCIAMACHY and SOLAR 2 brightness temperatures agree up to 1500 nm; above 1500 nm the noise does not permit a precise estimate of the agreement. However, between 1500 and 2400 nm, the brightness-temperature derived from SOLAR 2 presents a difference that reaches 300 K with the temperature brightness derived from the theoretical models and 450 K with the derived temperature from the ATLAS 3 spectrum.

This difference is not compatible with the TSI value. Therefore we integrated the spectra between 1000 and 1761 nm (the highest wavelength of SCIAMACHY). The brightness-temperature differences induce a change in the power contained in this spectral domain (Table 6).

SOLAR 2 and SCIAMACHY present a deficit close to 10 Wm^{-2} compared with the measured spectra ATLAS 3 (or WHI and SOLAR 1 *per* construction) and the COSI and SRPM modelled spectra. This difference is not compatible with the accuracy of the TSI ($\approx 10^{-3}$) or the TSI difference (4.5 Wm^{-2}) between the *Variability of solar IRradiance and Gravity Oscillations* (VIRGO) onboard SOHO (Fröhlich, 2012) and the *Total Irradiance Monitor* (TIM) onboard SORCE (Kopp and Lean, 2011).

Similarly to the temperatures yielded by COSI (Figure 12), the brightness-temperatures of the quiet Sun calculated with SRPM are up to 150 K lower than the measured temperature (Fontenla *et al.*, 2011). This 150 K difference might be an indication that the temperature structure of the low photosphere used to calculate the spectra needs to be slightly readjusted. However, the change of the temperature in the low photosphere will also affect the visible part of the spectrum, which currently agrees very well with the measurements (see *e.g.* Figure 11) because the formation regions of the visible and infrared irradiance overlap, which makes readjusting the temperature structure a challenge. While it can potentially solve the problem, another reason for the difference between theoretical and observed spectra may be the general limitations of the 1D models for the solar irradiance. The temperature bifurcations may reach up to 600 K in the low photosphere (Socas-Navarro, 2011). These temperature bifurcations may potentially be responsible for the 5 % deviation in the infrared spectrum. For example, Uitenbroek and Criscuoli (2011) showed that calculations with a single 1D temperature structure cannot reproduce the irradiance over the entire solar spectrum with equal accuracy.

4. Conclusion

The ISS-SOLAR measurements are the first with an in-orbit recalibration capability for the total spectral range of interest. To retain the accuracy determined on ground in space, on-

board means are essential to monitor the inherent temporal efficiency changes of the space instrumentation. In the EUV spectral range, SolACES used ionization chambers that are considered a primary detector standard. Within SOLSPEC, several sources allowed us to check the instrument stability. Furthermore, instrument characterization in space was discussed in detail.

In August 2009, the EUV data showed a distinct minimum during the extended solar minimum period between Solar Cycles 23 and 24, while at UV wavelengths this minimum appeared before this time. These data were presented in this article.

Using SolACES, SOLSPEC, and SOLSTICE SSI to fill the spectral gap between the two first instruments, we built two spectra, SOLAR 1 and SOLAR 2, which differ between 1100 and 2400 nm where we used ATLAS 3 in SOLAR 1. In this spectral range, SOLAR 2 showed a lower SSI, reaching 10 % at 1700 nm. An exhaustive investigation was carried out with the aim to understand this difference. However, no explanation was found, and this study is still in progress.

An important aspect of SSI measurements is the validation/comparison with the theoretical models. We used the results from the COSI and SPRM models. Several comparisons between ATLAS 3, SOLAR, WHI, and theoretical spectra showed an overall agreement, taking into account the uncertainties of these spectra. However, in some small wavelength domains, the differences (expressed in terms of percentages) were not compatible with the combined uncertainties of each compared spectrum. These cases were explained either by a low signal-to-noise ratio, instrument uncertainties, or by limitations in the lines list used to simulate the solar spectrum. These spectra were used to derive the temperature of the solar atmosphere. Up to 1100 nm, these temperatures agreed within 50 K. Above 1100 nm, the measured spectra provided consistent temperatures; but these were higher than the theoretical derived temperatures by up to 150 K. In contrast, the SOLAR 2 spectrum provided temperature lower by 450 K than the temperature derived from the other experimental spectra. It is expected that the SCIAMACHY data processing will improve the SSI IR part, and that the investigations of the IR SOLSPEC spectrometer will continue to study the SSI difference between SOLAR 1 and SOLAR 2.

The new calibration method of SolACES was successfully achieved in space for the first time. Applying this technique to future solar missions will offer an important opportunity to significantly increase the radiometric accuracy of the EUV-SSI data. A common feature between SolACES and SOLSPEC is the existence of calibration means in space. Nevertheless, we cannot exclude the occurrence of incidents (*e.g.* the loss of the deuterium lamp power supply) and ageing in orbit. However, implementing redundant means would allow us to devise solutions based on specific measurements and operation modes.

Acknowledgements We thank the referee for his or her pertinent review and his or her suggestion to use the SRPM model in this study. This investigation is supported by the Centre National d'Etudes Spatiales (France), the Centre National de la Recherche Scientifique (France), the Federal Office for Scientific, Technical and Cultural Affairs (Belgium), and the Bundesministerium für Forschung und Technologie (Germany). The participating institutes are the Service d'Aéronomie du CNRS, now LATMOS, the Institut d'Aéronomie Spatiale de Belgique, the Fraunhofer Institute for Physical Measuring Technique (Freiburg), and the Landessternwarte of Heidelberg. The SOLSPEC and SolACES absolute calibrations have been carried out with the blackbody BB3200g from the Physikalisch-Technische Bundesanstalt (PTB, Braunschweig, Germany), and SURF BESSY II (PTB, Berlin, Germany), respectively. SOLAR and SolACES constitute an external payload of the ESA *Columbus* laboratory placed onboard the *International Space Station*. The SOLAR operations are conducted by the Belgium User Support Operations Center (B-USOC) via the *Columbus* Control Center of DLR (Oberpfaffenhofen, Germany). SolACES has been developed by the Fraunhofer IPM. EADS Astrium Friedrichshafen supported the institute in performing the qualification and documentation. The project was sponsored by DLR, ESA, and the Fraunhofer Gesellschaft. A.I. Shapiro is supported by the Swiss National Science Foundation under grant CRS1122-130642 (FUPSOL). We are happy to thank J. Harder for providing

the SIM data used in this article. The research leading to these results has received funding from the European Community's Seventh Framework Programme (FP7 2012) under grant agreement n° 313188 (SOLID).

References

- Bolsée, D.: 2012, PhD Thesis, Univ. Bruxelles.
- Bovensmann, H., Burrows, J.P., Buchwitz, M., Frerick, J., Noel, S., Rozanof, V.V., Chance, K.V., Goede, A.P.H.: 1999, *J. Atmos. Sci.* **56**, 127. doi:[10.1175/1520-0469](https://doi.org/10.1175/1520-0469).
- Busa, I., Andretta, V., Gomez, M.T., Terranegra, L.: 2001, *Astron. Astrophys.* **373**, 993B. doi:[10.1051/0004-6361:20010661](https://doi.org/10.1051/0004-6361:20010661).
- Crotser, D.A., Woods, T.N., Eparvier, F.G., Triplett, M.A., Woodraska, D.L.: 2007, In: Fineschi, S., Viereck, R.A. (eds.) *SPIE CS-6689*. doi:[10.1117/12.732592](https://doi.org/10.1117/12.732592).
- DeLand, M.T., Cebula, R.P.: 1998, *Solar Phys.* **177**, 117. doi:[10.1023/A:1004931218139](https://doi.org/10.1023/A:1004931218139).
- Fontenla, J., White, O.R., Fox, P.A., Avrett, E.H., Kurucz, R.L.: 1999, *Astrophys. J.* **518**, 480. doi:[10.1086/307258](https://doi.org/10.1086/307258).
- Fontenla, J.M., Avrett, E., Thuillier, G., Harder, J.: 2006, *Astrophys. J.* **639**(1), 441. doi:[10.1086/499345](https://doi.org/10.1086/499345).
- Fontenla, J.M., Curdt, W., Haberreiter, M., Harder, J., Tian, H.: 2009, *Astrophys. J.* **707**, 482. doi:[10.1088/0004-637X/707/1/482](https://doi.org/10.1088/0004-637X/707/1/482).
- Fontenla, J.M., Harder, J., Livingston, W., Snow, M., Woods, T.: 2011, *J. Geophys. Res.* **116**, D20108. doi:[10.1029/2011JD016032](https://doi.org/10.1029/2011JD016032).
- Fröhlich, C.: 2012, *Surv. Geophys.* **33**, 453. doi:[10.1007/s10712-011-9168](https://doi.org/10.1007/s10712-011-9168).
- Haberreiter, M., Schmutz, W., Hubeny, I.: 2008, *Astron. Astrophys.* **492**, 833. doi:[10.1051/00046361:200809503](https://doi.org/10.1051/00046361:200809503).
- Harder, J.W., Thuillier, G., Richard, E.C., Brown, S.W., Lykke, K.R., Snow, M., McClintock, W.E., Fontenla, J.M., Woods, T.N., Pilewskie, P.: 2010, *Solar Phys.* **263**(1–2), 3. doi:[10.1007/s11207-010-9555-y](https://doi.org/10.1007/s11207-010-9555-y).
- Kopp, G., Lean, J.L.: 2011, *Geophys. Res. Lett.* **38**, L01706. doi:[10.1029/2010GL045777](https://doi.org/10.1029/2010GL045777).
- Meehl, G.A., Tebaldi, C., Walton, G., Easterling, D., McDaniel, L.: 2009, *Geophys. Res. Lett.* **36**(23), L23701. doi:[10.1029/2009GL040736](https://doi.org/10.1029/2009GL040736).
- Mihalas, D.: 1978, *Stellar Atmospheres*, Freeman, San Francisco, 102.
- Nikutowski, B., Brunner, R., Erhardt, Ch., Knecht, St., Schmidtke, G.: 2011, *Adv. Space Res.* **48**, 899. doi:[10.1016/j.asr.2011.05.002](https://doi.org/10.1016/j.asr.2011.05.002).
- Paganan, J., Harder, J.W., Weber, M., Floyd, L.F., Burrows, J.P.: 2011, *Astron. Astrophys.* **528**, A67. doi:[10.1051/0004-6361/201015632](https://doi.org/10.1051/0004-6361/201015632).
- Rottman, G.J.: 2005, *Solar Phys.* **230**(1), 7. doi:[10.1007/s11207-005-8112-6](https://doi.org/10.1007/s11207-005-8112-6).
- Schmidtke, G., Fröhlich, C., Thuillier, G.: 2006, *Adv. Space Res.* **37**(2), 255. doi:[10.1016/j.asr.2005.01.009](https://doi.org/10.1016/j.asr.2005.01.009).
- Schmidtke, G., Brunner, R., Eberhard, D., Halford, B., Klocke, U., Knothe, M., Konz, W., Riedel, W.-J., Wolf, H.: 2006, *Adv. Space Res.* **37**, 273. doi:[10.1016/j.asr.2005.01.112](https://doi.org/10.1016/j.asr.2005.01.112).
- Schmidtke, G., Nikutowski, B., Jacobi, Ch., Brunner, R., Erhardt, Ch., Knecht, S., Scherle, J., Schlagenhauf, J.: 2013, *Solar Phys.*, in press. doi:[10.1007/s11207-013-0430-5](https://doi.org/10.1007/s11207-013-0430-5).
- Schmutz, W., Fehlmann, A., Hülsen, G., Meindl, P., Winkler, R., Thuillier, G., Blattner, P., et al.: 2009, *Metrologia* **46**, S202. doi:[10.1088/0026-1394/46/4/S13](https://doi.org/10.1088/0026-1394/46/4/S13).
- Shapiro, A.I., Schmutz, W., Schoell, M., Haberreiter, M., Rozanov, E.: 2010, *Astron. Astrophys.* **517**, A48. doi:[10.1051/0004-6361/200913987](https://doi.org/10.1051/0004-6361/200913987).
- Shapiro, A.I., Schmutz, W., Dominique, M., Shapiro, A.V.: 2013, *Solar Phys.* **286**, 271. doi:[10.1007/s11207-012-0063-0](https://doi.org/10.1007/s11207-012-0063-0).
- Short, C.I., Hauschildt, P.H.: 2009, *Astrophys. J.* **691**, 1634. doi:[10.1088/0004-637X/691/2/1634](https://doi.org/10.1088/0004-637X/691/2/1634).
- Snow, M., McClintock, W.E., Woods, T.N., White, O.R., Harder, J.W., Rottman, G.: 2005a, *Solar Phys.* **230**, 325. doi:[10.1007/s11207-005-6879-0](https://doi.org/10.1007/s11207-005-6879-0).
- Snow, M., McClintock, W.E., Rottman, G., Woods, T.N.: 2005b, *Solar Phys.* **230**, 295. doi:[10.1007/s11207-005-8763-3](https://doi.org/10.1007/s11207-005-8763-3).
- Socas-Navarro, H.: 2011, *Astron. Astrophys.* **529**, A37. doi:[10.1051/0004-6361/201015805](https://doi.org/10.1051/0004-6361/201015805).
- Thuillier, G., Floyd, L., Woods, T.N., Cebula, R., Hilsenrath, E., Hersé, M., Labs, D.: 2004, In: Pap, J., Fox, P. (eds.) *Solar Variability and Its Effect on Climate, AGU Monogr.* **141**, 171. doi:[10.1029/141GM13](https://doi.org/10.1029/141GM13).
- Thuillier, G., Foujols, T., Bolsée, D., Gillotay, D., Hersé, M., Peetermans, W., Decuyper, W., Mandel, H., Sperfeld, P., Pape, S., Taubert, D.R., Hartmann, J.: 2009, *Solar Phys.* **257**(1), 185. doi:[10.1007/s11207-009-9361-6](https://doi.org/10.1007/s11207-009-9361-6).
- Thuillier, G., DeLand, M., Shapiro, A., Schmutz, W., Bolsée, D., Melo, S.M.L.: 2012, *Solar Phys.* **277**, 245. doi:[10.1007/s11207-011-9912-5](https://doi.org/10.1007/s11207-011-9912-5).
- Uitenbroek, H., Criscuolo, S.: 2011, *Astrophys. J.* **736**, 69. doi:[10.1088/0004-637X/736/1/69](https://doi.org/10.1088/0004-637X/736/1/69).

- Viereck, R.A., Floyd, L.E., Crane, P.C., Woods, T.N., Knapp, B.G., Rottman, G., Weber, M., Puga, L.C., DeLand, M.T.: 2004, *Space Weather* **2**, S10005. doi:[10.1029/2004SW000084](https://doi.org/10.1029/2004SW000084).
- White, O., Kopp, G., Snow, M., Tapping, K.: 2011, *Solar Phys.* **274**(1–2), 159. doi:[10.1007/s11207-010-9680-7](https://doi.org/10.1007/s11207-010-9680-7).
- Woods, T.N., Eparvier, F.G., Bailey, S.M., Chamberlin, Ph.C., Lean, J., Rottman, G.J., Solomon, S.C., Tobiska, W.K., Woodraska, D.L.: 2005, *J. Geophys. Res.* **110**(A1), A01312. doi:[10.1029/2004JA010765](https://doi.org/10.1029/2004JA010765).
- Woods, T.N., Chamberlin, P.C., Harder, J.W., Hock, R.A., Snow, M., Eparvier, F.G., Fontenla, J., McClintock, W.E., Richard, E.C.: 2009, *Geophys. Res. Lett.* **36**(1), L01101. doi:[10.1029/2008GL036373](https://doi.org/10.1029/2008GL036373).
- Woods, T.N., Eparvier, F.G., Hock, R., Jones, A.R., Woodraska, D., Judge, D., Didkovsky, L., Lean, J., Mariska, J., Warren, H., McMullin, D., Chamberlin, P., Berthiaume, G., Bailey, S., Fuller-Rowell, T., Sojka, J., Tobiska, W.K., Viereck, R.: 2010, *Solar Phys.* **275**(1–2), 115. doi:[10.1007/s11207-009-9487-6](https://doi.org/10.1007/s11207-009-9487-6).
- Worden, J., Schmidtke, G., Doll, H.G., Solomon, S.C.: 1996, *Opt. Eng.* **35**(2), 554.